

Coherence measures for heralded single-photon sources

E. Bocquillon,^{1,2} C. Couteau,¹ M. Razavi,^{3,*} R. Laflamme,^{1,4} and G. Weihs¹

¹*Institute for Quantum Computing and Department of Physics and Astronomy,
University of Waterloo, 200 University Ave W., Waterloo, ON, Canada N2L 3G1*

²*Ecole Normale Supérieure, 45, rue d'Ulm, 75230 Paris, France*

³*Institute for Quantum Computing and Department of Electrical and Computer Engineering,
University of Waterloo, 200 University Ave W., Waterloo, ON, Canada N2L 3G1*

⁴*Perimeter Institute for Theoretical Physics, 31 Caroline Street N., Waterloo, ON, Canada N2L 2Y5*

Single-photon sources (SPSs) are mainly characterized by the minimum value of their second-order coherence function, viz. their $g^{(2)}$ function. A precise measurement of $g^{(2)}$ may, however, require high time-resolution devices, in whose absence, only time-averaged measurements are accessible. These time-averaged measures, standing alone, do not carry sufficient information for proper characterization of SPSs. Here, we develop a theory, corroborated by an experiment, that allows us to scrutinize the coherence properties of heralded SPSs that rely on continuous-wave parametric down-conversion. Our proposed measures and analysis enable proper standardization of such SPSs.

PACS numbers: 42.50.Dv, 42.50.Ar, 42.65.Lm, 03.67.Dd

The demand for ultra-secure communication, high-precision measurement, and super-efficient computation [1] has resulted in the emergence of optical sources that create single—and, ideally, only single—photons in a heralding and/or on demand way [2]. The rapid progress in this area has been followed by its early introduction to the commercial market [3], even before finalizing a proper set of standards for characterizing such devices. For a heralded single-photon source (HSPS) that relies on the spontaneous parametric down-conversion (SPDC), where the detection of idler photons heralds for the presence of signal photons, two figures of merit are generally of crucial importance. The first is the temporal correlation between the signal and idler beams [4], on which our heralding mechanism relies, and the second is the second-order degree of coherence for the heralded signal photons [5]. The challenge of measuring either of these figures lies in the large bandwidth of the SPDC process, thereby the very narrow widths of such correlation functions. In fact, what we can commonly measure in an experimental setup is only a time-averaged version of the actual figure. It is important then to recognize all major parameters that affect our measurement results, and put them together to come up with well-defined, and readily measurable, figures of merit for HSPSs. This Report carves into the theoretical aspects of such problems and addresses the above coherence measures, and their corresponding time-averaged figures, with an accuracy never presented before. Our analysis accounts for the contribution of multi-photon states in the SPDC process as a function of pump power, or, effectively, the single-photon generation rate, for different widths of the coincidence window and photodetectors' time resolutions. Our theoretical predictions are corroborated by our experimental results, and they together provide a prescription for proper characterization of HSPSs.

Figure 1 shows the setup of our HSPS along with the

Hanbury Brown and Twiss (HBT) interferometer used for the measurement of the coherence function. In our experiment, a 405 nm continuous-wave laser pumped a periodically poled KTiOPO_4 (PPKTP) crystal. The crystal from Raicol was cut to $10 \times 2 \times 1 \text{ mm}^3$ for propagation along the x axis and poled with a $10 \mu\text{m}$ period to support type-II SPDC, where signal and idler photons have orthogonal polarizations. By using an oven, frequency degeneracy was reached at 39°C with a stability of $\pm 0.1^\circ\text{C}$. A polarizing beam splitter (PBS) split the two beams into two different spatial modes. A photodetection event on the idler beam heralded the presence of one or more photons on the signal beam, which went through an HBT interferometer consisting of a 50:50 beam splitter followed by two bandpass filters (810 nm, 10 nm bandwidth) and multi-mode fibers that coupled the light to photodetectors. We employed single-photon counting modules from Perkin-Elmer with nominal dead-times of 45 ns. Typical measured photon count rate for our setup was up to 800,000 counts/s in the idler channel, with a signal-idler coincidence rate amounting up to 10% of that value.

The detection times for the signal and idler beams were recorded by a time-tagging unit from Dotfast Consulting with a nominal temporal resolution of 156.25 ps. The time-tagging unit streamed the time tags to a computer, by which we could record single, double, and triple detection events between the three channels, i , s_1 , and s_2 , in Fig. 1. Coincidence windows were implemented only in software. The complete system of photodetectors, power supplies, time-stamping electronics, and the USB interface fit in a $30 \times 30 \times 30 \text{ cm}^3$ box.

The first coherence measure studied here is the temporal correlation between signal and idler beams, as a measure of reliability of our heralding mechanism, and is defined as follows

$$g_{si}^{(2)}(t, \tau) \equiv \frac{\langle \hat{E}_s^\dagger(t + \tau) \hat{E}_i^\dagger(t) \hat{E}_i(t) \hat{E}_s(t + \tau) \rangle}{\langle \hat{E}_s^\dagger(t + \tau) \hat{E}_s(t + \tau) \rangle \langle \hat{E}_i^\dagger(t) \hat{E}_i(t) \rangle}, \quad (1)$$

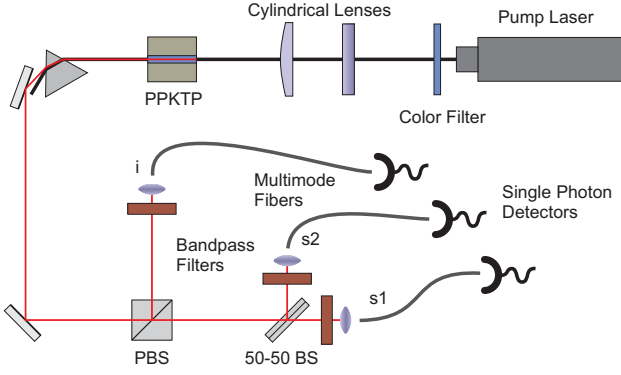


FIG. 1: (Color online) Experimental setup for our heralded single-photon source. A blue laser is cleaned from infrared fluorescence by a color filter, is focused by cylindrical lenses onto a PPKTP crystal (cut and poled for type-II), and is then removed from the down-converted beam by a dispersive prism. A polarizing beam splitter (PBS) splits the down-converted beam into the signal and idler arms. The idler beam i is used as a trigger and, in an HBT interferometer, the signal beam is split by a 50:50 beam splitter into $s1$ and $s2$ for the coherence function measurement. Bandpass filters block background light from entering the multi-mode fibers that couple the light to the single-photon detectors.

where $\hat{E}_s(t)$ and $\hat{E}_i(t)$ represent the scalar photon-units positive-frequency field operators for the outgoing signal (s) and idler (i) beams, respectively. The joint state of signal and idler is a zero-mean Gaussian state whose only nonzero second-order moments are given by [6]

$$e^{i\omega_p\tau/2}R(\tau) \equiv \langle \hat{E}_k^\dagger(t+\tau)\hat{E}_k(t) \rangle, \quad k = s, i, \quad (2)$$

$$e^{-i\omega_p(t+\tau)/2}C(\tau) \equiv \langle \hat{E}_s(t+\tau)\hat{E}_i(t) \rangle, \quad (3)$$

which represent the auto-correlation function and the phase-sensitive cross-correlation function between signal and idler fields, respectively, and where ω_p is the pump frequency. All other moments can be obtained by using the quantum form of the Gaussian moment-factoring theorem [7]. For instance, the numerator in Eq. (1) can be simplified as follows

$$\begin{aligned} P_{si}(\tau) &\equiv \langle \hat{E}_s^\dagger(t+\tau)\hat{E}_i^\dagger(t)\hat{E}_i(t)\hat{E}_s(t+\tau) \rangle \\ &= \langle \hat{E}_s^\dagger(t+\tau)\hat{E}_i^\dagger(t) \rangle \langle \hat{E}_i(t)\hat{E}_s(t+\tau) \rangle \\ &+ \langle \hat{E}_s^\dagger(t+\tau)\hat{E}_i^\dagger(t) \rangle \langle \hat{E}_i^\dagger(t)\hat{E}_s(t+\tau) \rangle \\ &+ \langle \hat{E}_s^\dagger(t+\tau)\hat{E}_s(t+\tau) \rangle \langle \hat{E}_i^\dagger(t)\hat{E}_i(t) \rangle \\ &= R^2(0) + |C(\tau)|^2, \end{aligned} \quad (4)$$

which represents the coincidence rate for having a signal photon at time $t+\tau$ and an idler photon at time t .

In the low-gain regime of parametric down-conversion, which prevails in our case, the auto- and cross-correlation functions can be approximated by the following expres-

sions [6]

$$R(\tau) = \begin{cases} R_{\text{SPDC}}(1 + \tau/\Delta t) & -\Delta t < \tau \leq 0 \\ R_{\text{SPDC}}(1 - \tau/\Delta t) & 0 < \tau \leq \Delta t \\ 0 & \text{elsewhere} \end{cases}, \quad (5)$$

where R_{SPDC} is the rate of photon generation for the signal/idler beam and $1/\Delta t$ is the bandwidth of the SPDC process, and

$$|C(\tau)| = \begin{cases} \sqrt{R_{\text{SPDC}}/\Delta t} & -\frac{\Delta t}{2} < \tau < \frac{\Delta t}{2} \\ 0 & \text{elsewhere} \end{cases}, \quad (6)$$

with the difference in the speed of light for ordinary and extraordinary axes in the crystal being compensated.

From Eqs. (1) and (4), we have $g_{si}^{(2)}(t, \tau) = 1 + |C(\tau)/R(0)|^2$. For our source, at 50 mW pump power, $R(0) = R_{\text{SPDC}} \approx 43$ MHz and $1/\Delta t \approx 3$ THz, which results in a peak value of $1 + 1/(\Delta t R_{\text{SPDC}}) \approx 7 \cdot 10^4$ for $g_{si}^{(2)}(t, \tau)$ at $\tau = 0$. The coherence function quickly drops to its minimum value one within a sub-picosecond period, however the finite time resolution in our experiment will smooth this feature out as we show next.

In order to measure $g_{si}^{(2)}(t, \tau)$, we approximate $P_{si}(\tau)$ by the rate of coincident events, $N_{si}(\tau)$, in which an idler photocount is observed at time t and a signal photocount is observed in the interval $[t+\tau-\tau_{\text{coin}}, t+\tau+\tau_{\text{coin}}]$, where $2\tau_{\text{coin}}$ is the width of our chosen coincidence window. Because of the photodetectors' time jitters, and neglecting dark counts throughout the Report, a photodetection event at time t only implies the existence of one or more photons in a neighborhood around time t . For simplicity, we assume that the detection time corresponding to a photon that hits the detector's surface at time t is uniformly distributed over the interval $[t-\tau_d, t+\tau_d]$, where τ_d is the time resolution of the photodetectors. We can then write the observed value for $N_{si}(\tau)$ in terms of $P_{si}(\tau)$ in the following way [8]

$$N_{si}(\tau) \approx \frac{1}{2\tau_{\text{coin}}} \int_{\tau-\tau_{\text{coin}}}^{\tau+\tau_{\text{coin}}} d\tau' \bar{P}_{si}(\tau'), \quad (7)$$

where

$$\bar{P}_{si}(\tau) = \int dt_i \int dt_s u(t_i)u(t_s - \tau)P_{si}(t_s - t_i) \quad (8)$$

is the coincidence rate for detecting a signal photon at time $t+\tau$ and an idler photon at time t , where $u(t) = 1/(2\tau_d)$ if $|t| \leq \tau_d$, and zero otherwise.

Figure 2 shows the experimental and the theoretical results for the time-averaged coherence function $\bar{g}_{si}^{(2)}(\tau) \equiv N_{si}(\tau)/R^2(0)$ for different values of τ_{coin} . Experimentally, $R^2(0)$ was determined by the product of the signal and idler count rates. For the theoretical graphs, we used the low-gain correlation functions given by Eqs. (5) and (6) with $R_{\text{SPDC}} = 43$ MHz and $1/\Delta t = 3$ THz. From Eqs. (6)–(8), we see that $N_{si}(\tau)$ has an almost fixed value

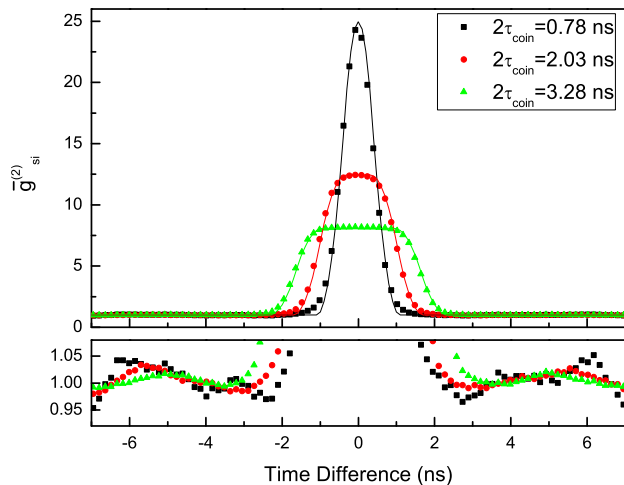


FIG. 2: (Color online) **Top:** Measurements (symbols) and theory predictions (lines) of the time-averaged coherence function $\bar{g}_{si}^{(2)}(\tau)$ for the signal and idler photons. The low-gain regime theory curves are in striking agreement with the data using the following parameter values $R_{\text{SPDC}} = 43$ MHz, $\tau_d = 350$ ps and $1/\Delta t = 3$ THz, where the last one was measured separately by spectroscopy and the other two were adapted to provide the subjective best visual fit simultaneously to all three sets of data. **Bottom:** Same data as top but with magnified ordinate in order to reveal structure that is caused by double reflection of photons from the fiber input endface and the surface of another optical element in the experiment. While this effect causes only very small deviations (0.2% of the central peak) from the expected flat line, these deviations cause noticeable ringing of the measured $\bar{g}_c^{(2)}$ (see Fig. 3).

for $\tau \in [-\tau_{\text{coin}} + \Delta t + \tau_d, \tau_{\text{coin}} - \Delta t - \tau_d]$, inversely proportional to τ_{coin} . As we get farther from the center, the time-averaged coherence function drops to its minimum value one as expected. The theoretical graphs are in striking agreement with our experimental results, which clearly demonstrate the strong temporal correlation between signal and idler beams.

The second coherence measure that we consider here is the degree of second-order coherence for the signal field, conditioned on observing an idler photocount at time t_i , defined as follows

$$g_c^{(2)}(t_1, t_2 | t_i) \equiv \frac{\langle \hat{E}_s^\dagger(t_1) \hat{E}_s^\dagger(t_2) \hat{E}_s(t_2) \hat{E}_s(t_1) \rangle_{\text{pm}}}{\langle \hat{E}_s^\dagger(t_1) \hat{E}_s(t_1) \rangle_{\text{pm}} \langle \hat{E}_s^\dagger(t_2) \hat{E}_s(t_2) \rangle_{\text{pm}}}, \quad (9)$$

where $\langle \cdot \rangle_{\text{pm}}$ is the average over the post-measurement state assuming sufficiently high time resolution and unity quantum efficiency for the idler photodetector.

To model the measurement on the idler field operator, we use a heuristic approach in which a photodetection event at time t_i on the idler beam is modeled by the measurement operator, [9], $\hat{E}_i(t_i)$. We can show that if we allow for infinitely high time resolutions this method provides us with the correct result [10]. The post-measurement averaging, for any operator \hat{X} , will

then be given by

$$\langle \hat{X} \rangle_{\text{pm}} = \langle \hat{E}_i^\dagger(t_i) \hat{X} \hat{E}_i(t_i) \rangle / \langle \hat{E}_i^\dagger(t_i) \hat{E}_i(t_i) \rangle. \quad (10)$$

The conditional coherence function in Eq. (9) can then be written as follows

$$g_c^{(2)}(t_1, t_2 | t_i) = \frac{P_{si}^{(2)}(t_1, t_2, t_i) R(0)}{P_{si}(t_1 - t_i) P_{si}(t_2 - t_i)}, \quad (11)$$

where, using the quantum version of the Gaussian moment-factoring theorem along with Eqs. (2) and (3),

$$\begin{aligned} P_{si}^{(2)}(t_1, t_2, t_i) &\equiv \langle \hat{E}_i^\dagger(t_i) \hat{E}_s^\dagger(t_1) \hat{E}_s^\dagger(t_2) \hat{E}_s(t_2) \hat{E}_s(t_1) \hat{E}_i(t_i) \rangle \\ &= R(0) [R^2(0) + |R(t_1 - t_2)|^2] \\ &\quad + 2\Re \{ C(t_1 - t_i) C^*(t_2 - t_i) R(t_1 - t_2) \} \\ &\quad + R(0) [|C(t_1 - t_i)|^2 + |C(t_2 - t_i)|^2] \end{aligned} \quad (12)$$

is the multi-coincidence rate for having signal photons at times t_1 and t_2 and an idler photon at t_i .

The first of several interesting special cases we consider is the coherence function at the trigger time, i.e.,

$$g_c^{(2)}(t_i, t_i | t_i) = 2 - \frac{2|C(0)|^4}{(R^2(0) + |C(0)|^2)^2}. \quad (13)$$

It is clear that if $R^2(0) \ll |C(0)|^2$ then $g_c^{(2)}(t_i, t_i | t_i) \approx 0$. This is the same requirement that we had for observing a large $g_{si}^{(2)}(t, 0)$ in Eq. (1), and, therefore, a low value for $g_c^{(2)}(t_i, t_i | t_i)$ is guaranteed if $g_{si}^{(2)}(t, 0) \gg 1$. The second interesting case is when $t_1 = t_i$ but $|t_2 - t_i| \gg 2\Delta t$. In this case, $g_c^{(2)}(t_i, t_2 | t_i) \approx 1$ provided that $R^2(t_2 - t_i) \approx 0$ and $|C^2(t_2 - t_i)| \approx 0$. This implies that our HSPS has a coherence time on the order of Δt . Finally, let us consider the case when $|t_1 - t_i = t_2 - t_i| \gg 2\Delta t$, i.e, when there is no correlation between the trigger time and the signal beam. In this case, $g_c^{(2)}(t_1, t_2 | t_i) \approx 2$, which is expected because, in the lack of any triggering event, both signal and idler beams individually obey the thermal-state statistics, for which the second-order coherence function has a maximum value of two [11].

To quantitatively characterize our HSPS, it is interesting to measure $g_c^{(2)}(\tau) \equiv g_c^{(2)}(t_i, t_i + \tau | t_i) = g_c^{(2)}(0, \tau | 0)$. For an ideal HSPS, we expect that $g_c^{(2)}(0) = 0$. In our case, from Eq. (13), $g_c^{(2)}(0) \approx 6 \cdot 10^{-5} \ll 1$. Here, we measure a time-averaged version of the coherence function by approximating $P_{si}(\tau)$ with $N_{si}(\tau)$ as before and $P_{si}^{(2)}(0, \tau, 0)$ with $N_{si}^{(2)}(\tau)$, the count rate for triple coincidences of an idler photodetection event at $t_i = 0$, and two signal photodetection events at $t_1 \in [-\tau_{\text{coin}}, \tau_{\text{coin}}]$ and $t_2 \in [\tau - \tau_{\text{coin}}, \tau + \tau_{\text{coin}}]$. In our HBT interferometer, we can equivalently look at the number of triple coincidences on the idler and s_1 - s_2 photodetectors. By accounting for the resolution of the three photodetectors

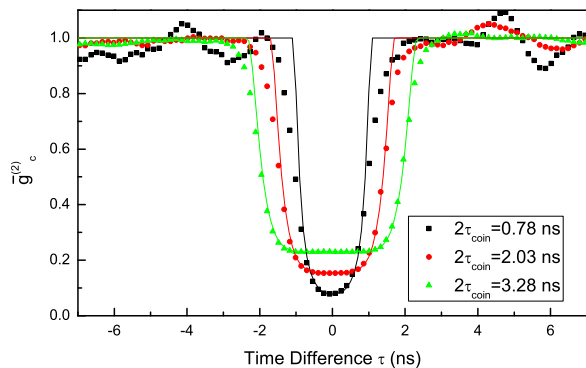


FIG. 3: (Color online) Measured (symbols) and calculated (lines) time-averaged conditional coherence function $\bar{g}_c^{(2)}(\tau)$. The theory lines were calculated using the same parameter values as in Fig. 2. The purely statistical errors of our data are on the order of the symbol size in the figure and therefore not shown. As explained in the caption of Fig. 2 photons that are reflected twice cause the apparent ringing.

involved in our measurement, we obtain [8]

$$N_{si}^{(2)}(\tau) = \frac{1}{(2\tau_{\text{coin}})^2} \int_{-\tau_{\text{coin}}}^{\tau_{\text{coin}}} dt_1 \int_{\tau-\tau_{\text{coin}}}^{\tau+\tau_{\text{coin}}} dt_2 \bar{P}_{si}^{(2)}(t_1, t_2, 0), \quad (14)$$

where

$$\begin{aligned} \bar{P}_{si}^{(2)}(t_1, t_2, 0) = & \int dt_i \int dt_{s_1} \int dt_{s_2} u(t_i) u(t_{s_1} - t_1) \\ & \times u(t_{s_2} - t_2) P_{si}^{(2)}(t_{s_1}, t_{s_2}, t_i) \end{aligned} \quad (15)$$

is the multi-coincidence rate for detecting an idler photon at time 0 and two signal photons at times t_1 and t_2 .

Figure 3 shows our measurement results for the time-averaged conditional coherence function $\bar{g}_c^{(2)}(\tau) \equiv N_{si}^{(2)}(\tau)R(0)/[N_{si}(0)N_{si}(\tau)]$ for three different coincidence windows, which result in three different widths for the observed central dip. Here, $R(0)$ is obtained from the idler count rate in the experiment. As explained in Fig. 2, the ringing structure in Fig. 3 is caused by double optical reflections. The graphs, nevertheless, exhibit the signature of a good SPS as the measured value of $\bar{g}_c^{(2)}(0)$, at 43 MHz single-photon generation rate, in Fig. 3, is 0.0781 ± 0.0006 for $2\tau_{\text{coin}} = 0.78$ ns and $\tau_d = 0.35$ ns. By reducing the pump power we can reduce this residual $\bar{g}_c^{(2)}(0)$ almost arbitrarily at the expense of reducing the total count rate. To see how the depth of the dip in Fig. 3 varies with the coincidence window, in Fig. 4, we have plotted $\bar{g}_c^{(2)}(0)$ versus $2\tau_{\text{coin}}$. It can be seen that, for $\tau_{\text{coin}} \ll \tau_d$, $\bar{g}_c^{(2)}(0)$ is determined by τ_d , whereas, for $\tau_{\text{coin}} \gg \tau_d$, it is almost linearly increasing with τ_{coin} . Our theoretical treatment is again well capable of reproducing the measurement results. The graph shown in Fig. 4 exemplifies the fact that a single value for $\bar{g}_c^{(2)}(0)$

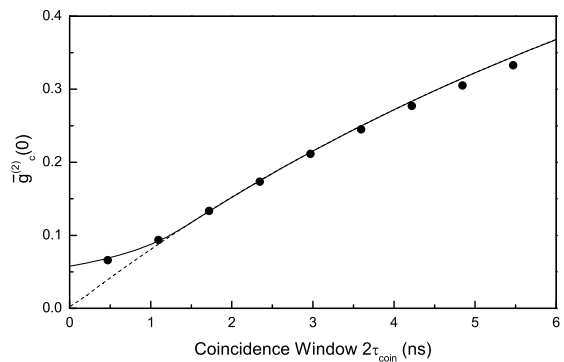


FIG. 4: (Color online) Experimental (symbols) and theoretical (line) results for the minimum of the time-averaged conditional coherence function, $\bar{g}_c^{(2)}(0)$, as a function of the coincidence window $2\tau_{\text{coin}}$ using the same set of parameters as in Fig. 2. The dashed line is for ideal photodetectors ($\tau_d = 0$).

does not bear enough information to quantify the source performance. At a fixed rate, the interplay between the coincidence window and the time resolution of photodetectors must also be accounted to give a proper figure of merit for an SPS.

In this Report, we theoretically and experimentally studied the coherence properties of heralded single-photon sources that use parametric down-conversion. We used the Gaussian characteristics of down-converted fields to analytically find the degree of second-order coherence between signal and idler fields as well as for the signal field, individually, when it is conditioned on the detection of an idler photon. Our theory is well capable of reproducing our experimental results, which demonstrated a high-quality source of sub-picosecond single photons. It also allowed us to study the impacts of the chosen coincidence window, the down-conversion parameters, and the resolution of photodetectors on the outcome. Such analysis enables proper standardization of such devices. We would like to thank N. Lütkenhaus, I. Söllner, and A. Safavi-Naeni for their technical assistance and acknowledge NSERC, CFI, ORF-RI, ORDCF, QuantumWorks, CIPI, and CIFAR for their financial support.

* Electronic address: mrazavi@iqc.ca

- [1] C. H. Bennett and G. Brassard, in *Proc. of IEEE Int. Conf. on Computer Syst. and Signal Process.* (IEEE, New-York, 1984), pp. 175-179; N. Sangouard *et al.*, *Phys. Rev. A* **76**, 050301(R) (2007); B. L. Higgins *et al.*, *Nature* **450**, 393 (2007); E. Knill *et al.*, *Nature* **409**, 46 (2001).
- [2] P. J. Mosley *et al.*, *Phys. Rev. Lett.* **100**, 133601 (2008); A. Trifonov *et al.*, *J. Opt. B: Quantum Semiclass. Opt.* **7**, S772 (2005); S. Fasel *et al.*, *New J. Phys.* **6**, 163 (2004); A. Soujaeff *et al.*, *Opt. Exp.* **15**, 726 (2007); S. A. Castelletto and R. E. Sholten, *Eur. Phys. J. AP* **41**, 181 (2008).
- [3] See, e.g., <http://qcvictoria.com>.

- [4] A. Valencia, M. V. Chekhova, A. Trifonov, and Y. Shih, *Phys. Rev. Lett.* **88**, 183601 (2002).
- [5] J. Rarity *et al.*, *Optics Communications* **62**, 201 (1987).
- [6] F. N. C. Wong, J. H. Shapiro, and T. Kim, *Laser Phys.* **16**, 1517 (2006).
- [7] J. H. Shapiro and K.-X. Sun, *J. Opt. Soc. Am. B* **11**, 1130 (1994).
- [8] Throughout the Letter, we assume unity quantum efficiencies for all employed photodetectors. Due to their normalized structures, coherence functions do not depend on photodetectors' quantum efficiencies.
- [9] M. A. Nielsen and I. L. Chuang, *Quantum Computation and Quantum Information* (Cambridge University Press, Cambridge, 2000).
- [10] M. Razavi *et al.*, to appear in *J. Phys. B*, special issue on Few-photon Optics (2009); eprint: quant-ph/0812.2445.
- [11] R. Loudon, *The Quantum Theory of Light* (Oxford University Press, Cambridge, 1983), 2nd ed.